Tuning Spin Hall Angles by Alloying

M. Obstbaum,[1] M. Decker,[1] A. K. Greitner,[1] M. Haertinger,[1] T. N. G. Meier,[1] M. Kronseder,[1] K. Chadova,[2] S. Wimmer,[2] D. Ködderitzsch,[2] H. Ebert,[2] and C. H. Back[1]

[1]*Institut für Experimentelle und Angewandte Physik, Universität Regensburg, 93040 Regensburg, Germany*

[2]*Department Chemie, Ludwig-Maximilians-Universität (LMU) München, 81377 Munich, Germany*

(Received 20 March 2016; revised manuscript received 16 September 2016; published 14 October 2016)

Within a combined experimental and theoretical study it is shown that the spin Hall angle of a substitutional alloy system can be continuously varied via its composition. For the alloy system Au_xPt_{1-x} a substantial increase of the maximum spin Hall angle compared to the pure alloy partners could be achieved this way. The experimental findings for the longitudinal charge conductivity σ, the transverse spin Hall conductivity σ_{SH}, and the spin Hall angle α_{SH} could be confirmed by calculations based on Kubo's linear response formalism. Calculations of these response quantities for different temperatures show that the divergent behavior of σ and σ_{SH} is rapidly suppressed with increasing temperature. As a consequence, σ_{SH} is dominated at higher temperatures by its intrinsic contribution that has only a rather weak temperature dependence.

DOI: 10.1103/PhysRevLett.117.167204

Magnetization switching in thin ferromagnetic films under the influence of spin transfer torques (STTs) [1–3] enables universal memory concepts. Focusing on ferromagnetic–normal-metal (FM-NM) bilayers, a pronounced STT on the magnetization of the FM can be achieved by utilizing the spin Hall effect (SHE) in the NM [4–6]. For that reason, the SHE and its inverse, i.e., the ISHE, have received a lot of interest over the last decade. In this context, many different experimental techniques have been applied to study the efficiency of the SHE in various NMs, with the corresponding figure of merit given by the spin Hall angle α_{SH}. When using a combination of electrical spin injection with nonlocal spin detection in the experiments [7–11], α_{SH} is usually defined as the ratio between the transverse (spin Hall) and the longitudinal conductivity of the NM, i.e., $\alpha_{SH} = \sigma_{SH}/\sigma$. Examining, on the other hand, in experiment the magnetization dynamics in the presence of STT and/or spin pumping [12–20], α_{SH} is defined via the ratio of generated to injected spin and charge currents, J_s and J_c, respectively. However, one should stress that the two different definitions of α_{SH} are fully consistent with each other as demonstrated, for example, in Ref. [21].

Concerning the charge to spin current conversion, the most efficient elemental NMs found so far are Pt, Pd, W, and Ta. Their spin Hall angles could be exceeded for some dilute alloys as for example Pt in Au [11] and Bi in Cu [10]. In these cases, the rather large observed spin Hall angles were ascribed to the skew scattering mechanism, although a reliable confirmation of this by means of numerically reliable *ab initio* electronic structure methods is by no means trivial [22].

Because of the complexity of the relativistic band structure of metals [23] and the ensuing transport properties [24], simple models are not capable of obtaining spin Hall angles in a material specific way. In recent years, efforts to calculate transverse transport properties from first principles succeeded in solving this task. Approaches calculating transverse transport properties with a formulation employing the Berry phase are able to describe perfect crystalline systems [25,26]. On the other hand, approaches employing the Boltzmann formalism [24,27], and Green function techniques that are used to solve the Kubo-Středa or Bastin transport equations [28] are able to treat disordered systems.

In this Letter we report on an experimental study on the ISHE in $Ni_{81}Fe_{19}/Au_xPt_{1-x}$ bilayers with the spin Hall angles α_{SH} determined for a wide range of composition. Our experimental findings that are confirmed by accompanying first principles calculations clearly show that α_{SH} can be tuned for Au_xPt_{1-x} over an extremely wide span with a pronounced maximum value for $x \approx 0.5$.

In our experimental setup (see Fig. 1), pure spin currents are injected via spin pumping [29–32] into Au_xPt_{1-x} by means of ferromagnetic resonance (FMR). To unambiguously extract voltage signals caused by the ISHE, the experimental approach already applied successfully to investigate pure Pt and Au on $Ni_{81}Fe_{19}$ [20] is used. A similar approach has been used by other authors to determine α_{SH} for $Ni_{81}Fe_{19}/Pt$ [19] who pointed out the reliability of the experimental method. By varying the angle ϕ_H between the static magnetization component and the attached voltage probes the contribution to the measured signal due to the anisotropic magnetoresistance (AMR) can be reliably separated from that due to the ISHE for the investigated $Ni_{81}Fe_{19}/Au_xPt_{1-x}$ bilayer systems. This way the voltage signals caused by the ISHE in the Au_xPt_{1-x} alloys can unambiguously be obtained. The subsequent determination of the spin Hall angle α_{SH} is performed by

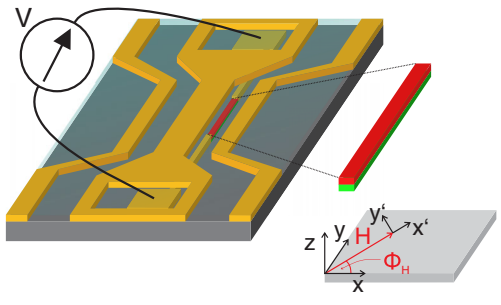

FIG. 1. Integration of a $Ni_{81}Fe_{19}/Au_xPt_{1-x}$-bilayer wire together with voltage probes in the experimental setup. The $Ni_{81}Fe_{19}$ layer is shown in green and the Au_xPt_{1-x} layer is shown in red. In this geometry the excitation field is perpendicular to the bilayer. The angle ϕ_H gives the angle between the voltage probes and the static magnetization. x', y', z define the local coordinate system of the magnetization.

fitting the pure ISHE voltage spectra at FMR to a Lorentzian line shape. Figure 2 shows a typical voltage trace for the $Ni_{81}Fe_{19}/Au_{0.47}Pt_{0.53}$ bilayer recorded for $\phi_H = 45°$ at a frequency of 12 GHz. Using the expressions (see Supplemental Material [33]) for the dc-voltage signals due to the AMR and the ISHE, V_{ISHE} and V_{AMR}, respectively, the measured voltage V can be split into a symmetric and antisymmetric part, as shown in Fig. 2. As the symmetric part at distinct angles stems only from the ISHE, one gets direct access to the corresponding spin Hall angle α_{SH} that is proportional to V_{ISHE}.

To quantify α_{SH} it is advantageous to keep the magnetization at $\phi_H = 0°$ allowing for a frequency dependent recording of the voltages V_{ISHE}^{oop}. In this case the formula for α_{SH} [15,20,34,35] reduces to

$$\alpha_{SH} = \frac{V_{ISHE}^{oop}\sigma(t_{NM}+t_{FM})M_S^2}{ef g_F^{\uparrow\downarrow}\Im(\chi_{z'z'}^{res})\chi_{y'z'}^{res}|h_z|^2 l\lambda_{sd}\tanh(\frac{t_{NM}}{2\lambda_{sd}})}, \quad (1)$$

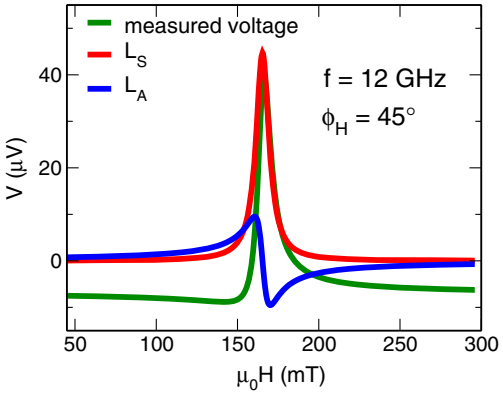

FIG. 2. Measured dc-voltage signal at FMR (green curve) for $\phi_H = 45°$ and a precession frequency of 12 GHz for a $Ni_{81}Fe_{19}/Au_{0.47}Pt_{0.53}$ bilayer. L_S and L_A denote the symmetric (red curve) and antisymmetric (blue curve), respectively, contribution according to a fit to a Lorentzian line shape.

where $\sigma(t_{NM}+t_{FM})$ is the conductivity of the bilayer system depending on the individual thicknesses t_{NM} and t_{FM}, respectively, M_S is the saturation magnetization of the FM film, $g_F^{\uparrow\downarrow}$ is the effective spin mixing conductance which contains the backflow correction, $\chi_{z'z'}^{res}$ and $\chi_{y'z}^{res}$ are elements of the Polder susceptibility tensor, l is the length of the wire and λ_{sd} is the spin diffusion length.

Obviously, the spin Hall angle depends on several parameters and their quantification is crucial for obtaining reliable results for α_{SH}. The effective spin mixing conductance $g_F^{\uparrow\downarrow}$ of the different $Ni_{81}Fe_{19}/Au_xPt_{1-x}$ interfaces is extracted from spin pumping experiments (again including the backflow correction) performed on corresponding calibration squares next to the wire. For this, the increase of the Gilbert damping constant α relative to the damping constant α_0 of uncapped $Ni_{81}Fe_{19}$ is used. For the data analysis it is assumed that the spin mixing conductance of the bilayer system $Ni_{81}Fe_{19}/Au_xPt_{1-x}$ decreases linearly with Au concentration x. This is well justified by measurements of $g_F^{\uparrow\downarrow}$ for various compositions (see Supplemental Material [33]). Most of the other magnetic parameters, including the susceptibility tensor elements, are determined on the basis of available data from experimental investigations on $Ni_{81}Fe_{19}/Au_xPt_{1-x}$ bilayers [36]. The excitation field h_z generated by the coplanar waveguide is estimated using electromagnetic simulation software and subsequent numerical evaluation. Since the spin diffusion length λ_{sd} enters Eq. (1) in an exponential manner, it is a crucial parameter concerning the determination of α_{SH}. In order to estimate λ_{sd} for all investigated Au_xPt_{1-x} alloys, V_{ISHE} has been measured as a function of the thickness for selected Au_xPt_{1-x}-layers. The analysis of the data (see Supplemental Material [33]) suggests that the λ_{sd} increases with increasing conductivity of the Au_xPt_{1-x} alloys (see Fig. 3 and Supplemental Material [33]). Using these data together with the measured value of $\lambda_{sd}(Pt) = 1.9$ nm for pure Pt, leads to the estimated values for λ_{sd} given in Fig. 3. For pure Au, $\lambda_{sd} = 34$ nm is assumed

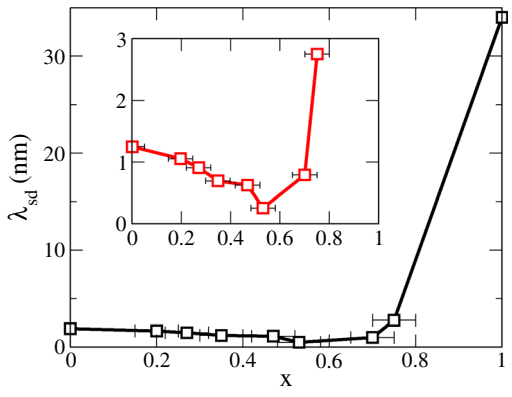

FIG. 3. Spin diffusion length λ_{sd}, of Au_xPt_{1-x} alloys determined assuming a linear dependence of λ_{sd} on the conductivity σ_{AuPt}. The inset shows λ_{sd} on an enlarged scale for the investigated concentration x below 0.8

[37]. Figure 3 shows that the spin diffusion length drops quickly when Pt is added to Au and that it is already comparable to the value for pure Pt for about 30% Pt in Au.

With a reliable estimate for the spin diffusion length available, the spin Hall angle α_{SH} of Au_xPt_{1-x} can finally be evaluated on the basis of Eq. (1), where σ stands for the conductivity of the complete $Ni_{81}Fe_{19}/Au_xPt_{1-x}$ bilayer (see Fig. 4 and Supplemental Material [33]). The corresponding values for α_{SH} are given in the top panel of Fig. 4 as a function of the composition. In particular, because of the

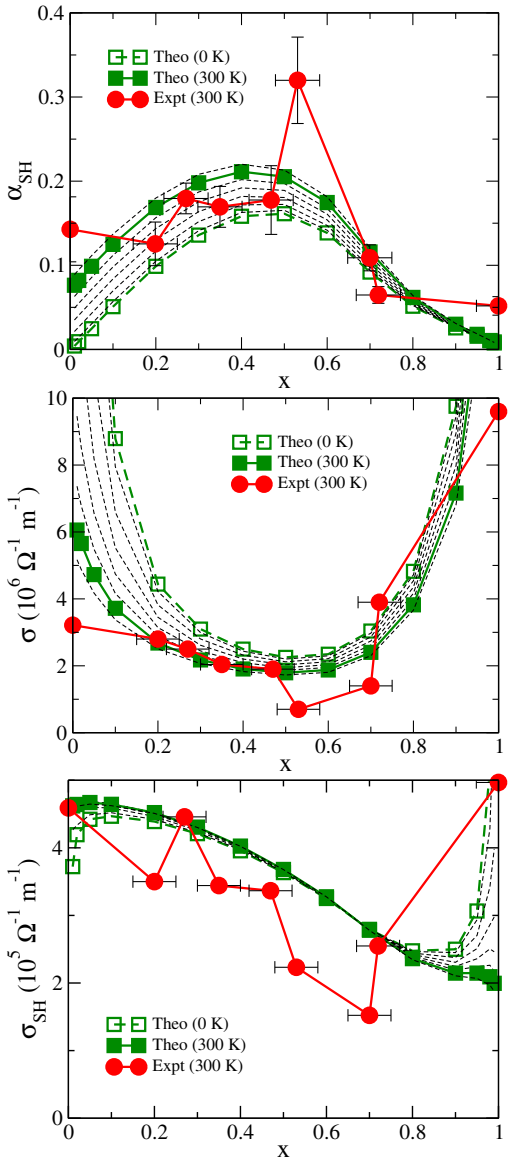

FIG. 4. Spin Hall angle α_{SH} (top), longitudinal charge conductivity σ (middle), transverse spin Hall conductivity σ_{SH} (bottom), of Au_xPt_{1-x} as a function of the concentration x. The full red circles give experimental data for $T = 300$ K, while the full (open) squares give results obtained using Kubo's linear response formalism in combination with the alloy analog model for $T = 300$ K ($T = 0$ K). The thin dashed lines give theoretical results for the temperature range between 0 and 350 K in steps of 50 K.

delicate dependence of α_{SH} on λ_{sd} as given by Eq. (1), the errors bars are relatively large. Nevertheless, it is obvious that α_{SH} for the concentrated alloys substantially exceeds the values for the pure components Pt and Au, respectively. This major experimental result of the present work clearly demonstrates that alloying and working with concentrated alloys opens a promising route to tune the spin Hall angle in a simple and robust way (see discussion below). Figure 4 gives the longitudinal charge conductivity σ (middle panel) of Au_xPt_{1-x} corresponding to the resistivity given in the Supplemental Material [33] and the transverse spin conductivity σ_{SH} (bottom panel) as deduced from α_{SH} and σ. As one notes, σ_{SH} varies for the considered composition regime nearly linearly with concentration x.

To support the interpretation of our experiments, *ab initio* investigations on the transport properties of Au_xPt_{1-x} alloys have been performed on the basis of Kubo's linear response formalism. These are based on a calculation of the underlying electronic structure by means of the KKR-GF (Korringa-Kohn-Rostoker Green function) method that gives direct access to the electronic GF. This allows us to account straightforwardly for random disorder in substitutional alloys by means of the coherent potential approximation (CPA). The CPA also offers a very reliable platform to deal with the so-called vertex corrections that occur when dealing with response functions. In the present case they give rise in particular to the extrinsic contribution to the spin Hall conductivity that is dominated by the skew scattering mechanism [28,38]. A most reliable treatment of this central spin-orbit induced transport property is ensured by using the fully relativistic formulation of the KKR-GF formalism [40]. For technical details see Ref. [41] and the Supplemental Material [33].

In contrast to previous theoretical work in the field, we accounted explicitly for the impact of finite temperatures on the transport properties. This is achieved by treating thermal lattice vibrations using the alloy analogy model [42]. Within this approach that is based on the adiabatic approximation, the temperature induced atomic displacements are seen as a random, quasistatic and temperature dependent distortion of the lattice with a corresponding distortion of the potential. The resulting temperature induced disorder of the potential is treated using the CPA as it is done for chemical disorder due to alloying.

The results for the longitudinal conductivity $\sigma(x, T)$ for $T = 0$ K given in Fig. 4 (middle, open squares) show as a prominent feature the typical divergent behavior $\sigma(x, 0) \approx \bar{\sigma}_{\mathrm{host(solute)}}/x_{\mathrm{solute}}$ in the dilute regime [43], where we find for the reduced conductivities $\bar{\sigma}_{\mathrm{Pt(Au)}} \lesssim \bar{\sigma}_{\mathrm{Au(Pt)}}$ [28], i.e., for Pt in Au and Au in Pt, respectively. This behavior reflects the fact that $\sigma(x, 0)$ for a perfectly periodic solid ($x = 0$ or 1) at $T = 0$ K becomes infinite and accordingly its resistivity becomes zero. On the other hand, for concentrations $0 < x < 1$ one has even for $T = 0$ K a finite conductivity corresponding to the residual resistivity. For finite

temperatures, $\sigma(x,T)$ becomes finite even in the case of pure elements due to electron-phonon scattering or, equivalently, thermally induced disorder [44]. As to be expected, because of the very different density of states at the Fermi energy, the corresponding conductivity drops much faster with temperature for pure Pt than for pure Au. For the dilute Au_xPt_{1-x} alloys with $x \lesssim 0.1$ or $x \gtrsim 0.9$, respectively, one finds $\sigma(x,T)$ also to be finite but one still notices a reminiscence of the divergence of $\sigma(x,0)$ for $x \to 0$ or 1, respectively. For the concentrated alloys ($0.2 \lesssim x \lesssim 0.8$), on the other hand, only a moderate change of about 20% for $\sigma(x,T)$ is found when going from $T = 0$ to 300 K. This implies that the scattering due to chemical disorder is more pronounced than that due to thermal lattice vibrations. Figure 4 (middle) shows that the calculations reproduce the experimental data for the conductivity σ measured at room temperature very well. This obviously also holds for the spin conductivity σ_{SH} that is given in Fig. 4 (bottom).

For the dilute regimes, the theoretical spin conductivity $\sigma_{SH}(x,T)$ also shows a $1/x_{solute}$ divergence reflecting that $\sigma_{SH}(x,T)$ is dominated by its skew scattering contribution $\sigma_{SH}^{skew}(x,T)$ as this scales for $T = 0$ K linearly with $\sigma(x,0)$ according to $\sigma_{SH}^{skew}(x,0) \approx S_{host(solute)}\sigma(x,0) = S_{host(solute)}\bar{\sigma}_{host(solute)}/x_{solute}$, where $S_{host(solute)}$ is the so-called skewness factor (see Supplemental Material [33]) [28,39,45]. Because $\bar{\sigma}_{Pt(Au)} \lesssim \bar{\sigma}_{Au(Pt)}$ and $S_{Pt(Au)} \approx -S_{Au(Pt)}/7.2$ [28] the divergent behavior of $\sigma_{SH}(x,0)$ is much more pronounced on the Au-rich side of the system than on the Pt-rich side. As found before for several other systems [28], one notes that the divergence leads to a strong increase of σ_{SH} on the Au-rich side while σ_{SH} decreases on the Pt-rich side for $x_{solute} \to 0$. This behavior again reflects the fact that the divergence is primarily due to the skew scattering (represented by the skewness factor S) with its magnitude and sign determined by the difference in the strength of the spin-orbit coupling for the host and solute atom [27]. As Fig. 4 shows, the divergent behavior of σ_{SH} in the dilute regime disappears very rapidly with rising temperature. In line with the behavior of σ, this change with temperature is much more pronounced for the Pt-rich than for the Au-rich side. For both sides of the system, however, the divergent behavior disappears completely at room temperature. In contrast to σ, the spin conductivity σ_{SH} shows only a very weak temperature dependence in the concentrated alloy regime. Further inspection of the theoretical results clearly shows that the extrinsic contributions to σ_{SH} connected with the vertex corrections hardly contribute in that regime. This means that the skew scattering mechanism can be ignored while the intrinsic contribution to σ_{SH} dominates. The data in Fig. 4 then imply in particular that the intrinsic contribution is essentially temperature independent as it is indeed found by the calculations (see Supplemental Material [33]).

Altogether, one notes that for the concentrated composition regime, Au_xPt_{1-x} shows the so-called *dirty* behavior [45] with negligible contributions to σ_{SH} due to the skew scattering mechanism and its intrinsic part dominating. This counterintuitive behavior was recently discussed in the context of the impact of chemical disorder on the anomalous Hall effect [46]. Here we find that not only chemical but also thermal disorder may drive a system into the dirty limiting behavior.

The spin Hall angle α_{SH} resulting from the calculated σ and σ_{SH} values is given in the top panel of Fig. 4. Because of the dependence of the individual conductivities on temperature and composition (see Supplemental Material [33]) one finds a very pronounced temperature dependence for α_{SH} on the Pt-rich side of the system that continuously gets diminished by alloying until it more or less disappears at the Au-rich end. This temperature dependence of α_{SH} for a given concentration x is primarily determined by that of σ as σ_{SH} depends rather weakly on T. In line with this, one finds that α_{SH} increases monotonically with temperature when x is kept fixed. Also the strongly asymmetric temperature dependence of α_{SH} is explained this way as the temperature dependence of σ is much more pronounced on the Pt-rich than on the Au-rich side of the system. Because of the pronounced minimum of σ that is located around $x \approx 0.5$ and the moderate concentration dependence of σ_{SH} one finds a clear maximum for α_{SH} more or less for the same alloy composition. Because of the very different temperature dependence of σ and σ_{SH} discussed, the maximum occurs for all temperatures with a weak shift towards pure Pt with increasing temperature. Finally, it should be noted that α_{SH} is not well defined in the case of pure systems ($x = 0$, or 1) at $T = 0$ K as σ becomes infinite (see Supplemental Material [33]). The corresponding limiting value $\alpha_{SH} \approx S_{host(solute)}$ for $x_{solute} \to 0$ to be expected from the properties of σ and σ_{SH} discussed above is obviously not yet reached for the compositions considered in Fig. 4 as the intrinsic contribution to σ_{SH} is that large (see Supplemental Material [33]).

In summary, it has been demonstrated that the FMR-based experimental setup used before to determine the spin Hall angle for pure elements can also be applied successfully for the investigation of substitutional alloy systems throughout the whole concentration regime. Working with concentrated alloys has the big advantage that one avoids the delicate dependence of the spin conductivity σ_{SH} on the concentration that is in general found for dilute alloys because of the divergent behavior of the skew scattering contribution. As it was demonstrated for the alloy system Au_xPt_{1-x}, it is nevertheless possible to surpass substantially the spin Hall angle α_{SH} of the pure components in the concentrated regime, i.e., to vary α_{SH} over a wide range via the concentration. All experimental findings could be quantitatively confirmed by the accompanying theoretical work based on Kubo's linear response formalism. As a new feature of such a type of calculations, the effect of finite temperatures could be accounted for. These calculations

clearly demonstrated that the divergent behavior of σ_{SH} in the dilute regime due to the skew scattering is rapidly suppressed with increasing temperature. For its intrinsic contribution, on the other hand, only a weak temperature dependence has been found.

Financial support by the DFG through the SFB 689 *Spin Phenomena in Reduced Dimensions* as well as SPP 1538 *Spin Caloric Transport* is gratefully acknowledged.

[1] L. Berger, Phys. Rev. B **54**, 9353 (1996).
[2] J. C. Slonczewski, J. Magn. Magn. Mater. **159**, L1 (1996).
[3] A. Brataas, A. D. Kent, and H. Ohno, Nat. Mater. **11**, 372 (2012).
[4] M. I. Dyakonov, Phys. Lett. **35A**, 459 (1971).
[5] J. E. Hirsch, Phys. Rev. Lett. **83**, 1834 (1999).
[6] K. Garello, I. M. Miron, C. O. Avci, F. Freimuth, Y. Mokrousov, S. Blügel, S. Auffret, O. Boulle, G. Gaudin, and P. Gambardella, Nat. Nanotechnol. **8**, 587 (2013).
[7] S. O. Valenzuela and M. Tinkham, Nature (London) **442**, 176 (2006).
[8] T. Kimura, Y. Otani, T. Sato, S. Takahashi, and S. Maekawa, Phys. Rev. Lett. **98**, 156601 (2007).
[9] T. Seki, I. Sugai, Y. Hasegawa, S. Mitani, and K. Takanashi, Solid State Commun. **150**, 496 (2010).
[10] Y. Niimi, Y. Kawanishi, D. H. Wei, C. Deranlot, H. X. Yang, M. Chshiev, T. Valet, A. Fert, and Y. Otani, Phys. Rev. Lett. **109**, 156602 (2012).
[11] B. Gu, I. Sugai, T. Ziman, G. Y. Guo, N. Nagaosa, T. Seki, K. Takanashi, and S. Maekawa, Phys. Rev. Lett. **105**, 216401 (2010).
[12] E. Saitoh, M. Ueda, H. Miyajima, and G. Tatara, Appl. Phys. Lett. **88**, 182509 (2006).
[13] K. Ando, S. Takahashi, K. Harii, K. Sasage, J. Ieda, S. Maekawa, and E. Saitoh, Phys. Rev. Lett. **101**, 036601 (2008).
[14] O. Mosendz, J. E. Pearson, F. Y. Fradin, G. E. W. Bauer, S. D. Bader, and A. Hoffmann, Phys. Rev. Lett. **104**, 046601 (2010).
[15] A. Azevedo, L. H. Vilela-Leão, R. L. Rodríguez-Suárez, A. F. Lacerda Santos, and S. M. Rezende, Phys. Rev. B **83**, 144402 (2011).
[16] L. Liu, T. Moriyama, D. C. Ralph, and R. A. Buhrman, Phys. Rev. Lett. **106**, 036601 (2011).
[17] L. Liu, C. F. Pai, Y. Li, H. W. Tseng, D. C. Ralph, and R. A. Buhrman, Science **336**, 555 (2012).
[18] C. F. Pai, L. Liu, Y. Li, H. W. Tseng, D. C. Ralph, and R. A. Buhrman, Appl. Phys. Lett. **101**, 122404 (2012).
[19] Z. Feng, J. Hu, L. Sun, B. You, D. Wu, J. Du, W. Zhang, A. Hu, Y. Yang, D. M. Tang, B. S. Zhang, and H. F. Ding, Phys. Rev. B **85**, 214423 (2012).
[20] M. Obstbaum, M. Härtinger, H. G. Bauer, T. Meier, F. Swientek, C. H. Back, and G. Woltersdorf, Phys. Rev. B **89**, 060407 (2014).
[21] L. Liu, R. A. Buhrmann, and D. C. Ralph, arXiv:1111.3702.
[22] D. V. Fedorov, C. Herschbach, A. Johansson, S. Ostanin, I. Mertig, M. Gradhand, K. Chadova, D. Ködderitzsch, and H. Ebert, Phys. Rev. B **88**, 085116 (2013).
[23] J. Sinova, S. O. Valenzuela, J. Wunderlich, C. H. Back, and T. Jungwirth, Rev. Mod. Phys. **87**, 1213 (2015).
[24] B. Zimmermann, K. Chadova, D. Ködderitzsch, S. Blügel, H. Ebert, D. V. Fedorov, N. H. Long, P. Mavropoulos, I. Mertig, Y. Mokrousov, and M. Gradhand, Phys. Rev. B **90**, 220403 (2014).
[25] G. Y. Guo, S. Murakami, T.-W. Chen, and N. Nagaosa, Phys. Rev. Lett. **100**, 096401 (2008).
[26] F. Freimuth, S. Blügel, and Y. Mokrousov, Phys. Rev. Lett. **105**, 246602 (2010).
[27] M. Gradhand, D. V. Fedorov, P. Zahn, and I. Mertig, Phys. Rev. Lett. **104**, 186403 (2010).
[28] S. Lowitzer, M. Gradhand, D. Ködderitzsch, D. V. Fedorov, I. Mertig, and H. Ebert, Phys. Rev. Lett. **106**, 056601 (2011).
[29] S. Mizukami, Y. Ando, and T. Miyazaki, J. Magn. Magn. Mater. **230**, 1640 (2001).
[30] B. Heinrich, Y. Tserkovnyak, G. Woltersdorf, A. Brataas, R. Urban, and G. E. W. Bauer, Phys. Rev. Lett. **90**, 187601 (2003).
[31] Y. Tserkovnyak, A. Brataas, and G. E. W. Bauer, Phys. Rev. Lett. **88**, 117601 (2002).
[32] Y. Tserkovnyak, A. Brataas, and G. E. W. Bauer, Phys. Rev. B **66**, 224403 (2002).
[33] See Supplemental Material at http://link.aps.org/supplemental/10.1103/PhysRevLett.117.167204 for more information on the experimental and theoretical background as well as additional supporting results.
[34] N. Mecking, Y. S. Gui, and C. M. Hu, Phys. Rev. B **76**, 224430 (2007).
[35] H. J. Jiao and G. E. W. Bauer, Phys. Rev. Lett. **110**, 217602 (2013).
[36] Z. Celinski, K. B. Urquhart, and B. Heinrich, J. Magn. Magn. Mater. **166**, 6 (1997).
[37] O. Mosendz, G. Woltersdorf, B. Kardasz, B. Heinrich, and C. H. Back, Phys. Rev. B **79**, 224412 (2009).
[38] For the sake of brevity, in the following we use the term *skew scattering* synonymously for all extrinsic contributions [27,39].
[39] K. Chadova, D. V. Fedorov, C. Herschbach, M. Gradhand, I. Mertig, D. Ködderitzsch, and H. Ebert, Phys. Rev. B **92**, 045120 (2015).
[40] H. Ebert, D. Ködderitzsch, and J. Minár, Rep. Prog. Phys. **74**, 096501 (2011).
[41] D. Ködderitzsch, K. Chadova, and H. Ebert, Phys. Rev. B **92**, 184415 (2015).
[42] H. Ebert, S. Mankovsky, K. Chadova, S. Polesya, J. Minár, and D. Ködderitzsch, Phys. Rev. B **91**, 165132 (2015).
[43] A. Crépieux and P. Bruno, Phys. Rev. B **64**, 014416 (2001).
[44] M. Jonson and G. D. Mahan, Phys. Rev. B **21**, 4223 (1980).
[45] N. Nagaosa, J. Sinova, S. Onoda, A. H. MacDonald, and N. P. Ong, Rev. Mod. Phys. **82**, 1539 (2010).
[46] R. Bianco, R. Resta, and I. Souza, Phys. Rev. B **90**, 125153 (2014).